A Low-carbon Operation Optimization Method of ETG-RIES Based on Adaptive Optimization Spiking Neural P Systems

Tao Wang, Zhu Huang, Ruixuan Ying, and Luis Valencia-Cabrera

***Abstract*—To enhance multi-energy complementarity and foster a low carbon economy of energy resources, this paper proposes an innovative low-carbon operation optimization method for electric-thermal-gas regional integrated energy systems. To bolster the low-carbon operation capabilities of such systems, a coordinated operation framework is presented that integrates carbon capture devices, power to gas equipment, combined heat and power units, and a multi-energy storage system. To address the challenge of high-dimensional constraint imbalance in the optimization process, a novel low-carbon operation optimization method is then proposed. The new method is based on an adaptive single-objective continuous optimization spiking neural P system, specifically designed for this purpose. Furthermore, simulation models of four typical schemes are established and employed to test and analyze the economy and carbon environmental pollution degree of the proposed system model, as well as the performance of the operation optimization method. Finally, simulation results show that the proposed method not only considers the economic viability of the target integrated energy system, but also significantly improves the wind power utilization and carbon reduction capabilities.**

***Index Terms*—Spiking neural P system, power-to-gas, membrane computing, regional integrated energy system, low-carbon operation optimization.**

Received: December 17, 2023
Accepted: July 26, 2024
Published Online: September 1, 2024

Tao Wang (corresponding author) is with the School of Electrical Engineering and Electronic Information, Xihua University, Chengdu 610039, China (e-mail: wangatao2005@163.com).

Zhu Huang is with the School of Electrical Engineering and Electronic Information, Xihua University, Chengdu 610039, China and the Xiluodu Hydropower Plant, China Yangtze Power Co., Ltd., Zhaotong 657300, China (e-mail: huangzhu_2019@163.com).

Ruixuan Ying is with the School of Electrical Engineering and Electronic Information, Xihua University, Chengdu 610039, China and the Institute of Multidisciplnary Research for Advanced Materials, Tohoku University, Sendai 980-8577, Japan (e-mail: yingruixuan123@gmail.com).

Luis Valencia-Cabrera is with the Department of Computer Science and Artificial Intelligence, University of Seville, Avda. Reina Mercedes s/n 41012, Spain (e-mail: lvalencia@us.es).

DOI: 10.23919/PCMP.2023.000208

I. Introduction

With the rapid development of the social economy, energy consumption is increasing sharply. Coal-fired thermal power continues to dominate in the energy structure in China, generating about 40% of total carbon dioxide (CO_2) emissions in the country [1]. The immense consumption of fossil fuels and the resultant environmental pollution in the power industry have exacerbated issues such as energy depletion and greenhouse effect. Economic indicators alone cannot be adapted to the current situation [2]. As a result, China has been vigorously pursuing the development of clean energy sources and actively exploring novel energy-utilization strategies to facilitate the transition to a low-carbon economy.

Regional integrated energy systems (RIESs) are capable of integrating a diverse array of resources, such as oil, natural gas and renewable energy sources. RIESs effectively realize the coordinated and complementary low-carbon operation of these multiple energy sources, making them a focal point of interest. Among the renewable energy sources, wind energy stands out as the most emblematic due to its clean and renewable nature [3]. Large-scale use of wind energy can effectively reduce the fossil energy consumption and the emission of CO_2 and other greenhouse gases [4]. However, the volatility and anti-peak regulation characteristics of wind power pose challenges to its development. This is particularly evident in northern China, where abundant wind and thermal energy resources coincide, leading to a pronounced issue of high wind power generation amidst low power consumption.

To address the issues, reference [5] investigates the impact of power to gas (P2G) technology in the integrated energy system. The study confirms that P2G technology can significantly promote wind power consumption as well as reduce fuel costs and CO_2 emissions. However, in this system, only the thermal generated by the combined heat and power (CHP) equipment supplies thermal energy to the thermal load, resulting in inadequate system flexibility. Reference [6] proposes an economic power dispatch model considering environmental costs. The model effectively mini-

mizes the emission of CO_2, SO_2 and other pollutant gases. However, it still regards CO_2 as an emission rather than a recyclable resources. While these systems have reduced CO_2 emissions, the coal-fired thermal power remains an active and flexible source in the integrated energy systems, emitting substantial amounts of CO_2 and other greenhouse gases. Consequently, how to manage this part of CO_2 remains an important issue of such research works.

As a result, researchers have proposed additional effective methods, such as carbon capture, utilization, and storage [7], [8]. Reference [9] combines the carbon capture and P2G technology to repurpose the CO_2 generated by cogeneration units in the synthesis of natural gas, and analyzes its impact on the economy and carbon emissions of the system. However, the system overlooks the energy consumption of carbon capture devices, which ultimately influences the emission analysis. To further reduce such CO_2 emissions and improve the utilization rate of wind power generation, reference [10] analyzes flexible operation modes for carbon capture and P2G equipment. However, the system neglects the utilization of energy storage devices, thereby limiting the flexibility of energy scheduling.

The main drawbacks of aforementioned works are summarized as follows. Either the energy consumption of equipment in the system is not fully considered, which can affect the overall assessment of the system economic viability, or the effective application of multi-energy storage is ignored. Actually, multi-energy storage can be used as a hub for the integration of different energy systems, thus improving the rigid connection between networks and realizing the decoupling of energy systems in time and space.

To mitigate carbon emissions from RIESs, improve the flexibility of energy dispatch and increase the utilization rate of wind power, this paper introduces a framework for an electric-thermal-gas regional integrated energy system that incorporates carbon capture devices. The corresponding mathematical model is described in detail, while multi-energy conversion technology and multi-energy storage system are considered to further enhance the flexibility of energy dispatch, fostering better coordination and complementarity within the system.

However, due to the increasing numbers of variables and high dimension of the proposed RIES, concerns about the computational efficiency and practical feasibility of the optimization process are raised, which pose a significant challenge. Various optimization algorithms have been commonly employed, such as particle swarm optimization algorithms (PSO) [11], genetic algorithms (GA) [12], grey wolf optimization (GWO) [13], or spiking neural P system (SNPS) [14], [15]. Among them, the SNPS is built based on the framework of membrane computing. In [14], a P system called optimization spiking neural P system (OSNPS) without evolutionary operators is constructed. The experimental results of OSNPS have advantages when compared with six other optimization algorithms by solving the same knapsack problem. In [15], a distributed adaptive spiking neural P system for solving combinatorial optimization problems is proposed. Experimental results demonstrate its effectiveness while experimental data analysis shows that the introduction of an adaptive learning rate and a distributed population structure significantly contributes to enhancing convergence and promoting population diversity. As evidenced by [14] and [15], SNPSs have proven to be both feasible and effective in solving such optimization problems.

Thus, in order to effectively solve the high-dimensional constraint imbalance problem in the optimization process of the RIES, we propose a novel low-carbon operation optimization method based on SNPSs. This proposed method is capable of adaptively adjusting mutation operators, so that it can be applied to large-scale practical optimization problems. The contributions of this paper are summarized as follows.

1) An optimal dispatch model of the electric-thermal-gas regional integrated energy system (ETG-RIES) is proposed. In the ETG-RIES, the CO_2 generated from different sources are utilized to the greatest extent possible, including carbon dioxide captured by carbon capture equipment and carbon dioxide supplied by manufacturers. Besides, the ETG-RIES combines a multi-element energy storage system (MESS) to shift energy temporally, to consume as much clean energy (e.g., wind energy) as possible, to reduce energy from coal-fired power plants, and to further reduce carbon dioxide emissions.

2) The proposed ETG-RIES is a high-dimensional model, and algorithms tend to get trapped in local optima when trying to find the optimal solution. Consequently, an adaptive single-objective continuous optimization spiking neural P system (ASCOSNPS) is designed, based on which the low-carbon operation optimization method of RIESs is proposed. Two special operators are designed in the proposed method, i.e., the cumulative mutation operator and the adaptive mutation operator. Consequently, the operation optimization method based on ASCOSNPS, in addition to its ability to escape from local optima, can also balance the contribution of the penalty function and avoid constraint imbalance.

3) The concept of carbon environment is introduced to assess the carbon reduction capability (CRC) of the ETG-RIES. The stronger the CRC of the ETG-RIES, the lower the degree of carbon environmental pollution.

The remainder of this paper is organized as follows. Section II presents the ETG-RIES framework and the models involving the most relevant equipment and devices. The optimal dispatch model and low-carbon operation optimization method of the ETG-RIES are

proposed in Section III and IV, respectively. The analysis of different case studies is provided in Section V, and a comparative analysis of the three algorithms provided is given in Section VI. Finally, conclusions are drawn in Section VII.

II. Regional Integrated Energy System

The proposed ETG-RIES is shown in Fig. 1, where CC denotes carbon capture, GT denotes gas turbine, EB denotes electric boiler, ESS denotes energy storage system, and TSS denotes thermal storage system. In the ETG-RIES, multi-element energy storage systems facilitate energy time-shift. Besides, the P2G, CHP and EB technologies enable multi-directional conversion of electric, thermal and gas energy. The CO_2 emissions from the power grid are recycled through the coupling of carbon capture devices and P2G equipment. Furthermore, CO_2 manufacturers are incentivized to supply additional CO_2 to the P2G equipment.

It is assumed that the power output from the grid is sourced primarily from coal-fired power plants. Moreover, for the purposes of clarity and calculation, all energy units have been standardized to power (kW). The system in Fig. 1 presents the key components that will be represented into the proposed mathematical models.

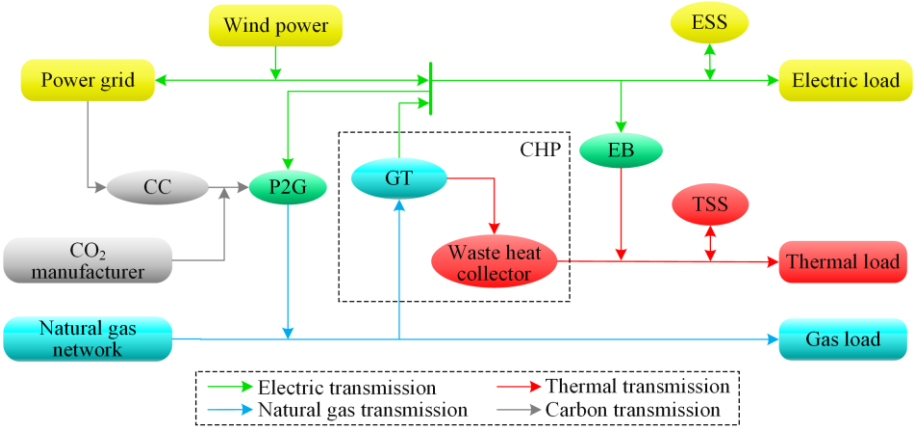

Fig. 1. Framework of electric-thermal-gas regional integrated energy system considering carbon capture devices.

A. P2G Model

There exist two kinds of P2G technologies, which are the power-to-hydrogen and power-to-gas. Given that the natural gas has a higher energy density per unit than hydrogen and can be seamlessly injected into existing natural gas networks for large-scale storage and long-distance transmissions [16], this paper primarily focuses on the power-to-gas process, which involves chemical reactions as illustrated in Fig. 2. In the first stage, oxygen and hydrogen molecules are produced in an electrolyzer. Subsequently, in the second stage, synthetic natural gas is generated in a Sabatier reactor, where hydrogen molecules react with CO_2 ones.

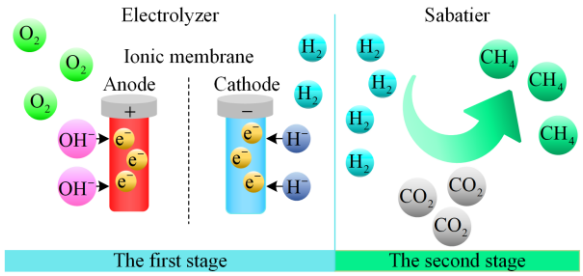

Fig. 2. Chemical reaction process of P2G.

The coupling relationships among electrical energy, natural gas and CO_2 are as follows:

$$P_{p2g}^{g}(t)=\eta_{p2g}P_{p2g}^{e}(t) \tag{1}$$

$$G_{c}(t)=\eta_{c}P_{p2g}^{g}(t) \tag{2}$$

where $P_{p2g}^{g}(t)$ represents the natural gas power of P2G at time t; while $P_{p2g}^{e}(t)$ and $G_{c}(t)$ represent the consumptions of electrical energy and CO_2 involved in the P2G process at time t, respectively; η_{p2g} represents the P2G efficiency; and η_{c} represents the CO_2 consumption coefficient of synthetic natural gas.

To ensure the stable operation of the P2G equipment, the aforementioned parameters should meet the following constraints:

$$P_{p2g}^{min}\leqslant P_{p2g}^{g}(t)\leqslant P_{p2g}^{max} \tag{3}$$

where P_{p2g}^{min} and P_{p2g}^{max} represent the minimum and maximum output power of the P2G equipment, respectively.

B. CHP Model

The CHP technology employs gas turbines to convert natural gas into electrical energy. Additionally, it utilizes waste heat recovery devices to harness the thermal energy produced alongside the electrical energy. Notably, this technology has comprehensive benefits, including energy savings, environment improvement, enhanced heating quality, and increased power supply [17].

Under the operation of the CHP system, the coupling relationships among the natural gas, electrical energy and thermal energy are as follows:

$$P_{\text{chp}}^{\text{e}}(t)=\eta_{\text{chp}}^{\text{e}}P_{\text{chp}}^{\text{g}}(t) \tag{4}$$

$$P_{\text{chp}}^{\text{h}}(t)=\eta_{\text{chp}}^{\text{h}}P_{\text{chp}}^{\text{g}}(t) \tag{5}$$

where $P_{\text{chp}}^{\text{e}}(t)$ and $P_{\text{chp}}^{\text{h}}(t)$ represent the electrical and heating power of the CHP equipment at time *t*, respectively; $P_{\text{chp}}^{\text{g}}(t)$ represents the natural gas consumption in the CHP process at time *t*; while $\eta_{\text{chp}}^{\text{e}}$ and $\eta_{\text{chp}}^{\text{h}}$ represent the electrical and thermal efficiencies of the CHP equipment, respectively.

To ensure the stable operation of the CHP equipment, the aforementioned parameters must adhere the following constraints:

$$P_{\text{chp}}^{\text{out}}(t)=P_{\text{chp}}^{\text{e}}(t)+P_{\text{chp}}^{\text{h}}(t) \tag{6}$$

$$P_{\text{chp}}^{\min}\leqslant P_{\text{chp}}^{\text{out}}(t)\leqslant P_{\text{chp}}^{\max} \tag{7}$$

where $P_{\text{chp}}^{\text{out}}(t)$ represents the total output power of the CHP equipment at time *t*; while $P_{\text{chp}}^{\min}$ and $P_{\text{chp}}^{\max}$ represent the minimum and maximum output power of the CHP equipment, respectively.

C. EB Model

The EB technology converts electrical energy into thermal energy for application to regional thermal loads. It not only promotes the consumption of wind power, but also breaks the traditional "ordering power based on thermal energy" model of cogeneration equipment.

The coupling relationship between electrical and thermal energy, facilitated by the EB technology, is as follows:

$$P_{\text{eb}}^{\text{h}}(t)=\eta_{\text{eb}}P_{\text{eb}}^{\text{e}}(t) \tag{8}$$

where $P_{\text{eb}}^{\text{h}}(t)$ and $P_{\text{eb}}^{\text{e}}(t)$ represent the heating power and power consumption of the EB at time *t*, respectively; whereas η_{eb} represents the EB efficiency.

To ensure the stable operation of the EB, the following constraint must be met for the involved parameters:

$$P_{\text{eb}}^{\min}\leqslant P_{\text{eb}}^{\text{h}}(t)\leqslant P_{\text{eb}}^{\max} \tag{9}$$

where $P_{\text{eb}}^{\min}$ and $P_{\text{eb}}^{\max}$ represent the minimum and maximum output power of EB, respectively.

D. Carbon Capture Model

The carbon capture technology is designed to capture the CO_2 emitted by power grids. The energy consumption of the carbon capture process is as follows:

$$P_{\text{oc}}(t)=\eta_{\text{c1}}W_{\text{c}}(t) \tag{10}$$

where $P_{\text{oc}}(t)$ represents the energy consumption of the carbon capture device at time *t*; η_{c1} represents the energy consumption coefficient of the carbon capture device; and $W_{\text{c}}(t)$ represents the amount of CO_2 captured by the carbon capture device at time *t*, given as:

$$W_{\text{c}}(t)=\eta_{\text{c2}}\eta_{\text{f}}P_{\text{p}\to\text{r}}(t) \tag{11}$$

where η_{c2} represents the carbon capture efficiency; η_{f} represents CO_2 generation coefficient of power grids; and $P_{\text{p}\to\text{r}}(t)$ represents the power output from the power grid to the ETG-RIES at time *t*.

E. General Model of Energy Storage Systems

Energy storage systems address discrepancies in energy supply and demand across both time and space. In the time dimension, energy storage systems transfer energy in different time periods. In the spatial dimension, energy storage systems can reduce energy output peaks and fill the trough of energy output. The integration of energy storage systems into RIESs significantly enhances the flexibility of the system.

The multi-element energy storage system discussed in this paper includes two primary components: ESS and TSS. Its generalized representation for charging and discharging processes is as follows:

$$P_{\text{ss}}(t)=\varepsilon P_{\text{ss,out}}(t)-(1-\varepsilon)P_{\text{ss,in}}(t) \tag{12}$$

where $P_{\text{ss}}(t)$, $P_{\text{ss,out}}(t)$ and $P_{\text{ss,in}}(t)$ represent the transmission energy, discharge power and charging power of the MESS at time *t*, respectively; ε represents the charging and discharging states of the MESS, whereas $\varepsilon=0$ means the MESS is in a charging state and $\varepsilon=1$ indicates a discharge state.

The energy stored by the MESS at time *t* is:

$$Q_{\text{ss}}(t)=Q_{\text{ss}}(t-1)-P_{\text{ss}}(t) \tag{13}$$

where $Q_{\text{ss}}(t-1)$ represents energy stored by the MESS at time $(t-1)$.

To ensure the stable operation of the MESS, the parameters involved should meet the following constraints:

$$0\leqslant P_{\text{ss,in}}(t)\leqslant P_{\text{c\_max}}^{\text{ss}} \tag{14}$$

$$0\leqslant P_{\text{ss,out}}(t)\leqslant P_{\text{s\_max}}^{\text{ss}} \tag{15}$$

$$Q_{\text{s\_min}}\leqslant Q_{\text{ss}}(t)\leqslant Q_{\text{s\_max}} \tag{16}$$

where $P_{\text{c\_max}}^{\text{ss}}$ and $P_{\text{s\_max}}^{\text{ss}}$ represent the maximum input and maximum output of the MESS, respectively; while $Q_{\text{s\_min}}$ and $Q_{\text{s\_max}}$ represent the minimum and maximum storage capacities of the MESS, respectively.

III. Optimal Dispatch Model of ETG-RIES

A. Objective Function

Considering the elements including the electrical energy interaction cost $C_{\text{p\_c}}$ between the ETG-RIES and the power grid, the natural gas purchase cost $C_{\text{g\_c}}$, the environmental cost $C_{\text{e\_c}}$ and the CO_2 purchase cost $C_{\text{buy\_c}}$, the objective function is established as:

$$f_{\min}=C_{\text{p\_c}}+C_{\text{g\_c}}+C_{\text{e\_c}}+C_{\text{buy\_c}} \tag{17}$$

where $f_{\min}$ represents the minimum economic cost of the energy dispatch of the ETG-RIES.

The electrical energy interaction cost between the ETG-RIES and power grid is as follows:

$$C_{\mathrm{p\_c}} = \sum_{t=1}^{T}\left(\lambda_{\mathrm{p}}(t)P_{\mathrm{p}\to\mathrm{r}}(t) - \lambda_{\mathrm{up}}(t)P_{\mathrm{r}\to\mathrm{p}}(t)\right) \tag{18}$$

where $\lambda_{\mathrm{p}}(t)$ and $\lambda_{\mathrm{up}}(t)$ represent the electricity purchase and sale prices at time t, respectively; $P_{\mathrm{r}\to\mathrm{p}}(t)$ represents the remaining power that is provided to the power grid; and T represents the operation cycle time of the ETG-RIES.

The natural gas purchase cost is:

$$C_{\mathrm{g\_c}} = \sum_{t=1}^{T}\lambda_{\mathrm{g}}P_{\mathrm{g}\to\mathrm{r}}(t) \tag{19}$$

where λ_{g} represents natural gas price; $P_{\mathrm{g}\to\mathrm{r}}(t)$ represents the amount of natural gas purchased by the RIES from the natural gas network at time t.

In this paper, the capture, storage and utilization technologies of CO_2 are employed to ensure that the park rarely emits CO_2 into the environment. Thus, the cost of CO_2 emission is ignored when calculating the total costs. To show simplicity and convenience, the capture and storage charges of CO_2 are called environmental cost in this paper, which is calculated by:

$$C_{\mathrm{e\_c}} = \sum_{t=1}^{T}\lambda_{\mathrm{p}}P_{\mathrm{oc}}(t) - \lambda_{\mathrm{c}}Q_{\mathrm{c}}(t),\ Q_{\mathrm{c}}(t) < 0 \tag{20}$$

$$Q_{\mathrm{c}}(t) = G_{\mathrm{c}}(t) - W_{\mathrm{c}}(t) \tag{21}$$

where λ_{c} represents the sequestration cost coefficient of CO_2; $Q_{\mathrm{c}}(t)$ represents the flow amount of CO_2. If $Q_{\mathrm{c}}(t) < 0$, then the ETG-RIES needs to store the excess of CO_2; otherwise, it needs to purchase Q_{c} kilogram of CO_2 from the CO_2 manufacturers.

The CO_2 purchase cost is:

$$C_{\mathrm{buy\_c}} = \tau_{\mathrm{c}}Q_{\mathrm{c}}(t),\ Q_{\mathrm{c}}(t) \geqslant 0 \tag{22}$$

where τ_{c} represents the cost coefficient of the ETG-RIES purchasing CO_2 from CO_2 manufacturers.

B. Power Balance Constraints

The expressions for the power balance constraints, which correspond to various power sources including electric, thermal and natural gas, are presented here.

1) Electric power balance constraint is as follows:

$$\begin{aligned} &P_{\mathrm{p}\to\mathrm{r}}(t) + P_{\mathrm{wind}}(t) + P^{\mathrm{e}}_{\mathrm{chp}}(t) + P_{\mathrm{ess}}(t) = \\ &P^{\mathrm{e}}_{\mathrm{load}}(t) + P^{\mathrm{e}}_{\mathrm{eb}}(t) + P^{\mathrm{e}}_{\mathrm{p2g}}(t) + P_{\mathrm{r}\to\mathrm{p}}(t) \end{aligned} \tag{23}$$

where $P_{\mathrm{wind}}(t)$ represents the output power of the wind power at time t; while $P_{\mathrm{ess}}(t)$ and $P^{\mathrm{e}}_{\mathrm{load}}(t)$ represent the power transmission of the ESS and regional electrical load at time t, respectively.

2) Thermal power balance constraint is as follows:

$$P^{\mathrm{h}}_{\mathrm{chp}}(t) + P^{\mathrm{h}}_{\mathrm{eb}}(t) + P_{\mathrm{tss}}(t) = P^{\mathrm{h}}_{\mathrm{load}}(t) \tag{24}$$

where $P_{\mathrm{tss}}(t)$ and $P^{\mathrm{h}}_{\mathrm{load}}(t)$ represent the thermal transmission of the TSS and regional thermal load at time t, respectively.

3) Natural gas power balance constraint is as follows:

$$P_{\mathrm{g}\to\mathrm{r}}(t) + P^{\mathrm{g}}_{\mathrm{p2g}}(t) = P^{\mathrm{g}}_{\mathrm{load}}(t) + P^{g}_{\mathrm{chp}}(t) \tag{25}$$

where $P^{\mathrm{g}}_{\mathrm{load}}(t)$ represents the regional gas load at time t.

IV. Low-carbon Operation Optimization Method of ETG-RIES

In this section, it first proposes the ASCOSNPS, and an ASCOSNPS-based operation optimization method for ETG-RIESs is then introduced. Following that, the algorithmic description of the proposed method is presented.

A. Adaptive Single-objective Continuous Optimization Spiking Neural P System

The OSNPS is first proposed in [14] in 2014. After a decade of development, several variants of OSNPS have been proposed [15]. However, these variants have primarily been used to solve discrete problems. Since the optimization problem we aim to solve is continuous, in this paper, we first refine the conventional OSNPS to adapt to the objective function at hand. As a result, the ASCOSNPS is presented.

Definition 1: An adaptive single-objective continuous optimization spiking neural P system (ASCOSNPS) of degree $m > 1$ is a tuple, i.e.: $\prod = (S_1, \cdots, S_m, G)$ where:

1) $S_l = (B, \sigma_1, \cdots, \sigma_{n+2}, syn, I_{\mathrm{out}}), 1 \leqslant l \leqslant m$, represents the ith subsystem, where:

i) $B = \{b\}$ represents a singleton alphabet, b represents a spike, and B represents a set of spikes;

ii) $Q = Q_p \bigcup Q_s$ represents a neuron set, while $Q_p = \{\sigma_1, \cdots, \sigma_n\}$ and $Q_s = \{\sigma_{n+1}, \sigma_{n+2}\}$ represent the sets of pulse-generating and pulse-supplying neurons, respectively. Each pulse-generating neuron σ_i is of the form $(\theta_i, R_i, P_i), 1 \leqslant i \leqslant n$, where:

a) θ_i represents the potential value of spikes contained in σ_i;

b) $R_i = \{a^{\theta} \to a^{\beta}\}$ represents the firing rule of σ_i, where its execution will consume a spike a^{θ} and generate a new pulse at the same time, denoted as a^{β};

c) P_i represents the rule excitation operator in σ_i;

iii) Both σ_{n+1} and σ_{n+2} work as the step-by-step supplier of spikes to $\sigma_1, \cdots, \sigma_n$;

iv) $syn = \{(i, j) \mid ((1 \leqslant i \leqslant n+1) \wedge (j = n++2)) \vee ((i = n+2) \wedge (j = n+1))\}$ represents the directional synaptic connection between neurons;

v) $I_{\text{out}} = \{\sigma_1, \cdots, \sigma_n\}$ represents a finite set of output neurons, i.e., the output is a spike train formed by concatenating the outputs of $\sigma_1, \cdots, \sigma_n$;

2) G represents an adaptive director, which is used to adaptively adjust the size of rule excitation operators in neuron σ_i.

B. ASCOSNPS-based Low-carbon Operation Optimization Method of ETG-RIES

In this section, the proposed ASCOSNPS is employed in the low-carbon operation optimization process of the ETG-RIES. The flow chart is shown in Fig. 3, where both $N_{\max}$ and $T_{\max}$ represent the maximum numbers of iterations, and *rand* represents a random number between 0 and 1.

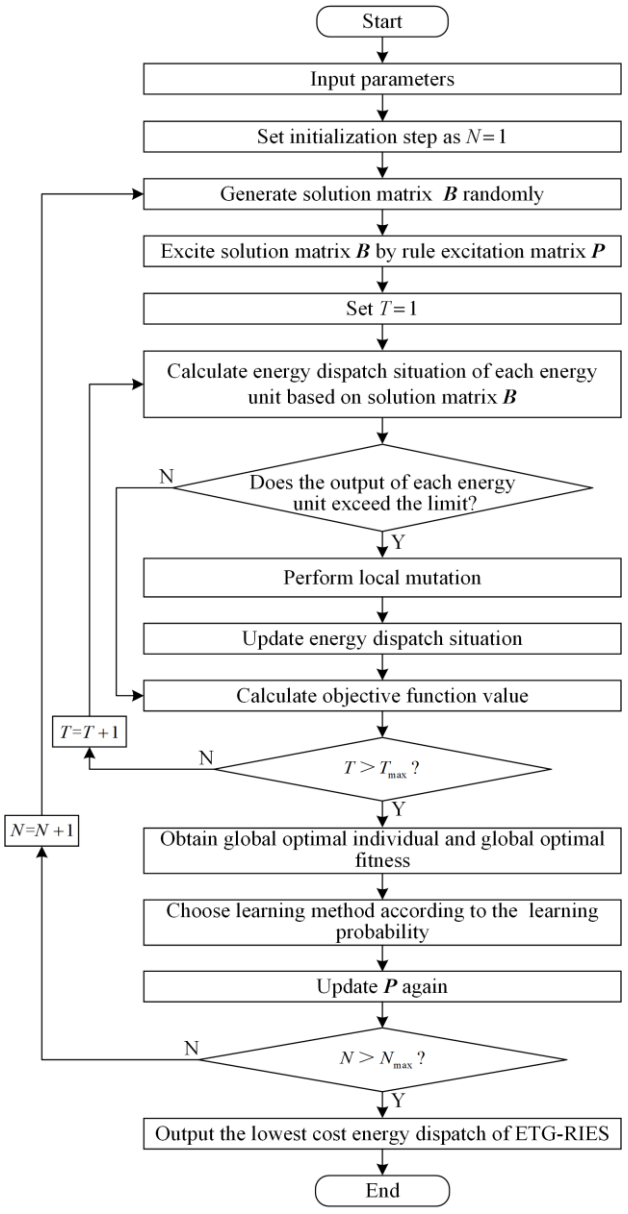

Fig. 3. Flow chart of low-carbon operation optimization method of ETG-RIES based on ASCOSNPS.

The steps of the proposed optimization method of ETG-RIES based on ASCOSNPS are described as follows.

Step 1: Input parameters. Input important parameters including electricity-heat-gas load, wind power output, energy prices and energy conversion efficiency of RIES, pulse sequence T_s, learning probability p_j^a, learning step ε and mutation operator v_1, v_2, v_3;

Step 2: Set the initial step N as 1;

Step 3: Generate the solution matrix ***B*** randomly;

Step 4: Excitation by rule matrix ***P***. Excite the solution matrix ***B*** by using the rule excitation matrix ***P***;

Step 5: Set the initialization step T of sub-loop as 1;

Step 6: Calculate energy dispatch. Based on the solution matrix ***B*** and the existing data and constraints in current area, calculate the energy dispatch situation for each energy unit;

Step 7: Check whether the output of each energy unit exceeds the limit. If the output does not exceed the limit, then go to Step 10; otherwise, proceed to Step 8;

Step 8: Perform local mutation. Generate cumulative gradient mutation operator to perform local mutation on contemporary solutions;

Step 9: Update energy dispatch. Update the energy dispatch situation for each energy unit and calculate the objective function value;

Step 10: Calculate the objective function value;

Step 11: if $T > T_{\max}$, then proceed to Step 12; otherwise, $T = T + 1$ and go to Step 6;

Step 12: Obtain the global optimal individual and global optimal fitness;

Step 13: Choose the learning method according to the learning probability;

Step 14: Update ***P*** again. Generate the mutation operators v_1 and v_2 to perform mutation operations on the rule excitation matrix ***P***, so as to update ***P*** again;

Step 15: Check whether the termination condition $N > N_{\max}$ is met. If so, then proceed to the Step 16; otherwise, $N = N + 1$ and go to Step 3 to continue the iteration;

Step 16: Output results and end computation. Output the lowest cost energy dispatch, including the optimal energy dispatch of each energy unit and the carbon emissions of the ETG-RIES. The algorithm execution is complete, and the computation ends.

The proposed method introduces three modules as shown in Figs. 4–6, namely, the cumulative gradient mutation module, learning module and adaptive mutation module. The goal of the approach is to improve the ability to solve high-dimensional optimization problems, increase the generalization ability and enhance the global optimization-seeking ability.

Specifically, the cumulative gradient mutation module performs probability accumulation for selective mutation based on the magnitude of the data, facilitating

compliance with the constraints of the operation optimization method. The learning module can randomly learn to update matrix $\boldsymbol{P}$, whereas the adaptive mutation module dynamically adjusts the mutation probability according to the iterative stage, thereby enhancing the global optimization-seeking.

The algorithmic elaboration of the proposed operation optimization method is as follows. This is the code for the main module, which is capable of calling module 1 and module 2.

Algorithm: ASCOSNPS-based operation optimization method

Input: electricity-thermal-gas load, wind power output, energy prices and energy conversion efficiency of the ETG-RIES, pulse sequence T_s, learning probability p_j^a, learning step ε and mutation operator v_1, v_2, v_3

1: Initialize individual optimal fitness and global optimal fitness, initialize mutation flag bit $u=1$, initialize mutation operator $v_1=0$, rearrange T_s into a regular excitation matrix, and initialize the solution matrix $\boldsymbol{P}=(p_{ij})_{H\times m}$
2: $gen=1$
3: while ($gen <$ Maxgen)
4: Generate solution matrix $\boldsymbol{B}=(b_{ij})_{H\times m}$
5: $\boldsymbol{B}=\boldsymbol{B}+(\boldsymbol{P}-\boldsymbol{B})/18$
6: Calculate the energy dispatch situation of each energy unit
7: Call module 1, update individuals
8: Update the energy dispatch situation of each energy unit
9: Calculate the objective function
10: Obtain the global optimal individual g^{b} and global optimal fitness g^{f}
11: $i=1$
12: while ($i=1:H$) **do**
13: while ($j=1:m$) **do**
14: Call module 2, update the rule excitation matrix *P*
15: Call module 3, update the rule excitation matrix *P* again
16: end while
17: end while
18: end while
Output: the lowest cost of output energy dispatch, the optimal energy dispatch of each energy unit and carbon emissions of the ETG-RIES

The cumulative gradient mutation operator v_3 in module 1 can balance the contribution of the penalty function and avoid the constraint imbalance problem. The flow chart of module 1 is shown in Fig. 4.

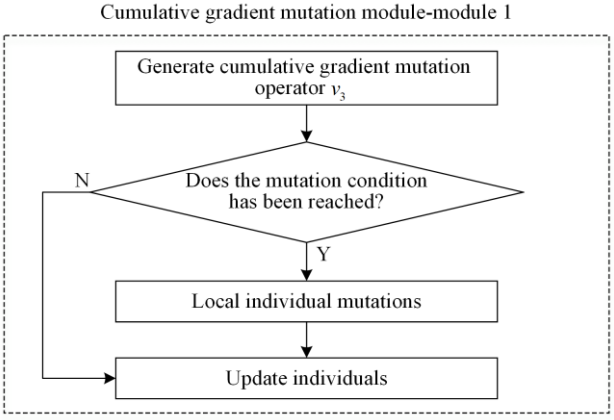

Fig. 4. Flow chart of cumulative gradient mutation module.

Module 1: Cumulative gradient mutation module

1: if $\frac{v_3}{2} > rand$ **then**
2: while ($t=1:ceil(m\times rand)$) **do**
3: $\boldsymbol{s}_t=g_{\mathrm{t}}^{\mathrm{b}}$
4: end while
5: end if

The individual mutation $\boldsymbol{s}_t$ occurs when the mutation condition is satisfied. The mutation module is shown as below, where $\boldsymbol{s}_t$ represents the tth ($1\leqslant t\leqslant m$) row vector in each generation of matrix $\boldsymbol{B}=(b_{ij})_{H\times m}$.

Let us note that the initial state of the mutation operator is $v_3=0$. Thus, when the constraint variable crosses the limit, the computational process is as follows:

$$v_3=v_3+v_{g\_i\_v} \tag{26}$$

where $v_{g\_i\_v}$ represents the vth step value of the ith constraint variable in the gth generation, where $1<g\leqslant$ Maxgen, $1\leqslant v\leqslant 3$, $1\leqslant i\leqslant m$.

After the previous steps are performed, the learning module start operating as follows.

Module 2: Learning module

1: if ($rand < p_j^a$) **then**
2: $k_1,k_2=ceil(rand\times H), k_1\neq k_2\neq i$
3: $x_j=x_{k_1}(f(x_{k_1})<f(x_{k_2}))+x_{k_2}(f(x_{k_1})>f(x_{k_2}))$
4: $p_{ij}=(p_{ij}+\varepsilon)(b_{ij}\oplus x_j)+(p_{ij}-\varepsilon)(\overline{b_{ij}\oplus x_j})$
5: else
6: if ($b_{ij}\neq g_{\mathrm{j}}^{\mathrm{b}}$) **then**
7: $p_{ij}=(p_{ij}+\varepsilon)(g_{\mathrm{j}}^{\mathrm{b}}<0.5)+(p_{ij}+\varepsilon)(g_{\mathrm{j}}^{\mathrm{b}}>0.5)$
8: end if
9: Over-limit processing for rule excitation operator p_{ij}
10: end if

The flow chart of module 2 is shown in Fig. 5.

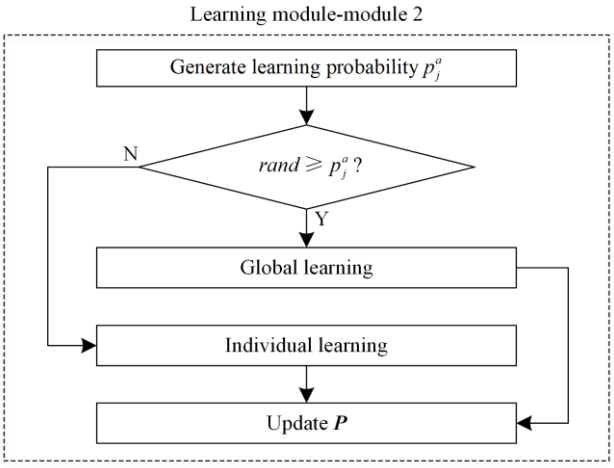

Fig. 5. Flow chart of learning module.

Since this single module alone cannot adequately handle the high dimensional problems, an adaptive

mutation operator (v_1, v_2) is added after module 2, which can dynamically scale the mutational range. Under the control of (v_1, v_2), the rule excitation matrix $\boldsymbol{P}$ has a high mutation probability in the early stages of the iteration. At the later stages, the mutation probability will become smaller and smaller, so as to avoid missing the global optimum.

The early stages of the adaptive mutation are shown in module 3-(1), while its later stages are shown in module 3-(2).

Module 3-(1): Early stages of the adaptive mutation

1: $u=1$
2: if ($gen < \frac{8\times \text{Max}gen}{10}$) **then**
3: **if** ($v_1 > 0.25$) **then**
4: $v_1 = 0.75$
5: **end if**
6: **if** ($rand < v_1$ and $rand > v_2$) **then**
7: **if** ($rand < 0.56$) **then**
8: **while** ($i = 1:H$) **do**
9: **while** ($j = 1:m$) **do**
10: **if** ($i \neq x$) **then**
11: $p_{ij} = rand$
12: **end if**
13: **end while**
14: **end while**
15: **end if**
16: $u=0$
17: **end if**
18: end if

Module 3-(2): Later stages of the adaptive mutation

1: if ($gen \geqslant \frac{8\times \text{Max}gen}{10}$) **then**
2: **if** ($rand < v_1$ *and* $rand > v_2$) **then**
3: **if** ($rand < 0.035$) **then**
4: **while** ($i = 1:H$) **do**
5: **while** ($j = 1:m$) **do**
6: **if** ($i \neq x$) **then**
7: $p_{ij} = rand$
8: else
9: continue
10: **end if**
11: **end while**
12: **end while**
13: **end if**
14: $u=0$
15: **end if**
16: end if

The generation process of v_1 and v_2 in the proposed adaptive mutation operator (v_1, v_2) is as follows:

$$v_1 = v_1 u + \frac{2}{gen} \tag{27}$$

where v_1 represents the iterative mutation accumulation value and u represents the mutation flag bit. If the mutation occurs, then $u=0$ and $v_1 = 0$; otherwise, $u=1$ and this state will remain until the next mutation happens.

$$v_2 = \frac{1}{\left(1+\exp\left(-\frac{1}{2}\times\frac{\log(D^{gen})}{\log(D^0)}\right)\right)\times 2} \tag{28}$$

where v_2 represents the difference variance ratio mapping value, which can be used to maintain the population diversity. D^{gen} represents the individual mean maximum difference in the contemporary population and is calculated by (29), while D^0 represents the individual mean maximum difference in the initial population and is calculated in a similar manner as D^{gen}.

$$D^{gen} = \frac{1}{m}\sum_{i=1}^{m}\left(\max\left(D_1^{gen}(:,i)\right)\right) \tag{29}$$

$$D_1^{gen} = \left|p_{im}^{gen} - p_{jm}^{gen}\right|, i\in[1,H-1],\ j\in[2,H] \tag{30}$$

where the D_1^{gen} represents the individual difference in the contemporary population.

The flow chart of module 3 is shown in Fig. 6.

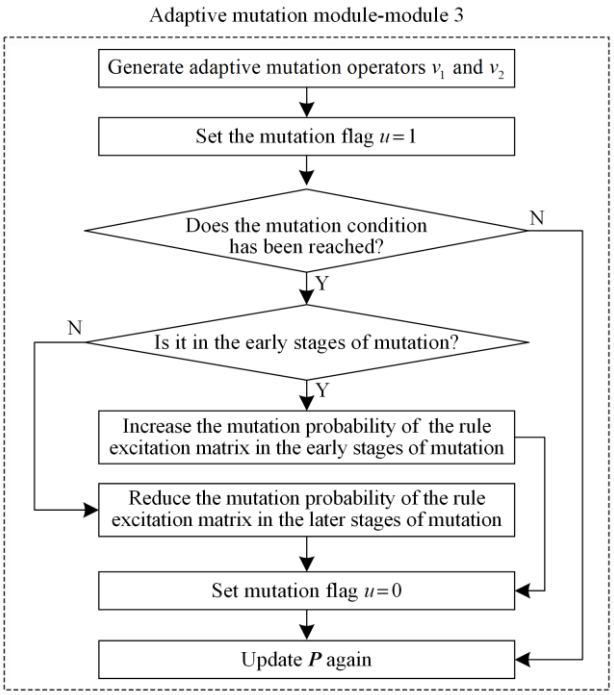

Fig. 6. Flow chart of adaptive mutation module.

V. Case Analysis

In this section, the proposed ASCOSNPS-based operation optimization method is employed to solve the models in Sections II and III. The problem to be solved has high-dimensional nature. Initially, the fundamental parameters are introduced, and the four cases are then compared to clarify the features included in each model. Finally, the effectiveness and superiority of the ASCOSNPS-based method in optimizing the operation of the proposed RIES are tested and verified.

A. Basic Parameters

We have selected a northern region as an illustrative example. The purchase and sale prices of electricity, as

well as the natural gas price are presented in Table I. Additionally, the ETG-RIES parameters are detailed in Table II [16], [18]–[26], while the load-side energy consumption and wind power data are depicted in Fig. 7. In Table II, Q_{ess} and Q_{tss} represent the storage capacities of the ESS and TSS, respectively.

TABLE I
ELECTRICITY AND NATURAL GAS PRICES

Time periods	Electricity purchase price (¥/kWh)	Electricity sale price (¥/kWh)	Natural gas price (¥/kWh)
Peak periods	0.84	0.65	0.258
Normal periods	0.62	0.47	0.258
Valley periods	0.42	0.33	0.258

Note: 10:00–15:00, 18:00–21:00 (peak periods); 07:00–10:00, 15:00–18:00, 21:00–23:00 (normal periods); 00:00–07:00, 23:00–24:00 (trough periods)

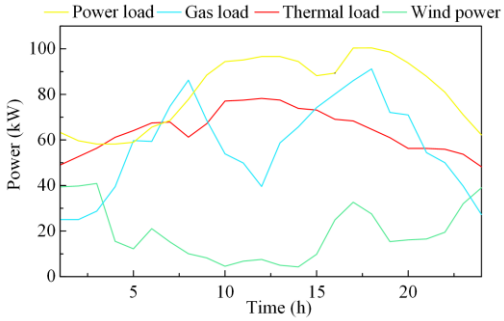

Fig. 7. Load-side energy consumption data and wind power data.

TABLE II
PARAMETERS OF THE ETG-RIES

Parameters	Value	Parameters	Value
τ_c (¥/kg)	0.5	η_g (kg/ kWh)	0.22
λ_c (¥ /kg)	0.03	P_{p2g}^{min} (kW)	0
η_f (kg/ kWh)	0.98	P_{p2g}^{max} (kW)	30
η_c (kg/ kWh)	0.2	P_{chp}^{min} (kW)	15
η_{eb} (%)	95	P_{chp}^{max} (kW)	115
η_{p2g} (%)	60	P_{eb}^{min} (kW)	0
η_{chp}^{e} (%)	40	P_{eb}^{max} (kW)	30
η_{chp}^{h} (%)	45	Q_{ess} (kWh)	120
η_{c2} (%)	90	Q_{tss} (kWh)	80
η_{c1} (kWh /kg)	0.269		

B. Cases Setting

To verify the effectiveness of the proposed model (Case 1), three other RIES frameworks (i.e., Cases 2–4 shown in Table III) are set up for simulation and analysis. The four cases are designed from the perspective of carbon reduction and improvement of wind energy utilization. The simulation results are analyzed from the aspects of the economy and carbon environmental pollution degree of the RIESs.

The energy dispatch results for Cases 1–4 are shown in Figs. 8–11, where the parts above and below the 0-scale line indicate the energy output and consumption of the equipment, respectively. The subgraphs (a)–(c) in Figs. 8–11 indicate the dispatching results corresponding to electrical energy, thermal energy and natural gas, respectively, for Cases 1–4. The wind power consumption rate by the RIESs under different cases are shown in Table IV, and the costs resulting from the daily energy consumption (calculated in kW) are shown in Table V. In addition, we employ the commercial solver CPLEX to solve the proposed model. Experiments results show that the cost by using CPLEX is 2043.2651 yuan per day, which is higher than the result (i.e., 1912.08 yuan per day) by using our proposed optimization method. Consequently, in comparison, ASCOSNPS demonstrates a higher cost-effectiveness in finding optimal solutions than CPLEX.

TABLE III
CONFIGURATION OF CASES 1–4

Cases	Carbon capture	Wind power	P2G	CHP	EB	ESS	TSS
1	√	√	√	√	√	√	√
2	√	√	√	√	√	×	×
3	×	√	√	√	√	√	√
4	√	√	×	√	√	√	√

Note: "×" indicates that there are no corresponding equipment.

C. Economic Comparison

In this section, the optimization outcomes of the four cases shown in Table III are presented. These results contain the energy dispatch details of each sub-equipment, the associated costs, and the wind power utilization rate.

TABLE IV
WIND POWER CONSUMPTION RATE BY RIESS UNDER EACH CASE

Cases	1	2	3	4
Wind power consumption rate (%)	100	98.03	98.00	92.45

TABLE V
COST RESULTS OF CASES 1–4

(¥/day)

Cases	Total cost	Electrical energy interaction cost	Natural gas purchase cost	Environmental cost	CO_2 purchase cost
1	1912.08	739.16	968.79	203.21	0.92
2	1952.06	754.46	989.57	207.91	0.12
3	1736.59	767.55	952.79	0	16.25
4	1720.08	572.62	1008.86	138.60	0

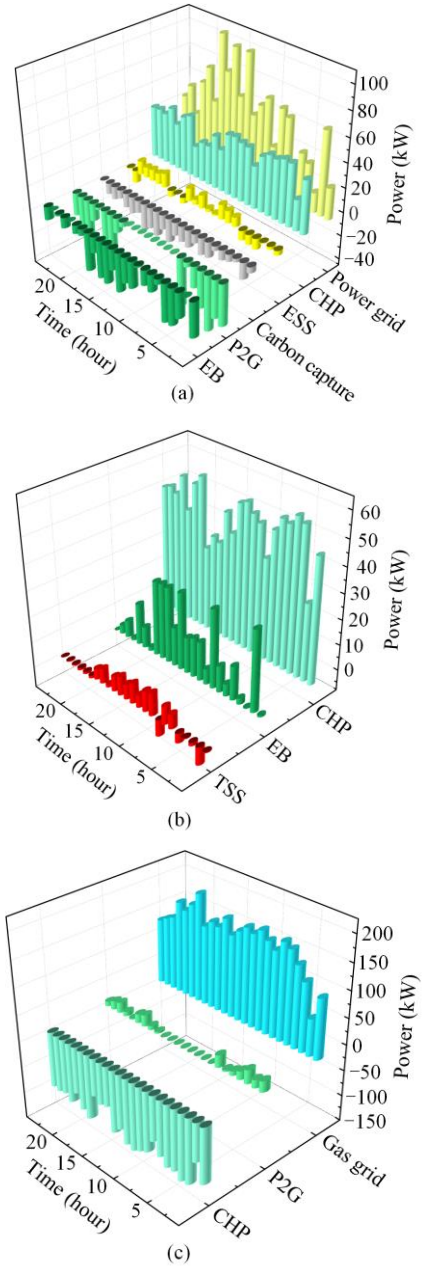

Fig. 8. Energy dispatch results in Case 1. (a) Electrical energy. (b) Thermal energy. (c) Natural gas.

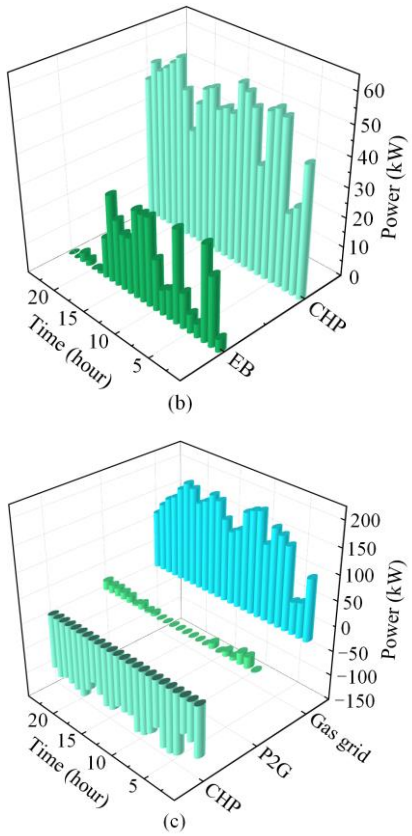

Fig. 9. Energy dispatch results in Case 2. (a) Electrical energy. (b) Thermal energy. (c) Natural gas.

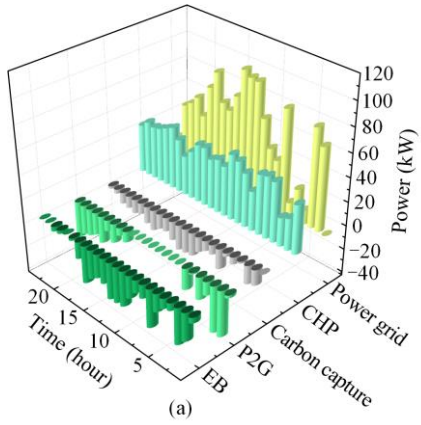

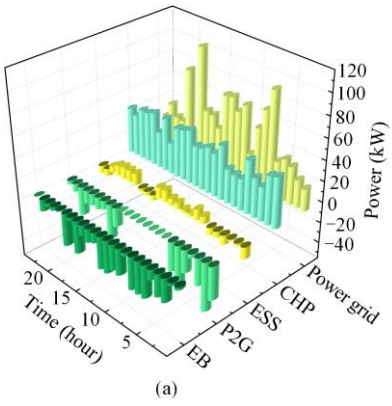

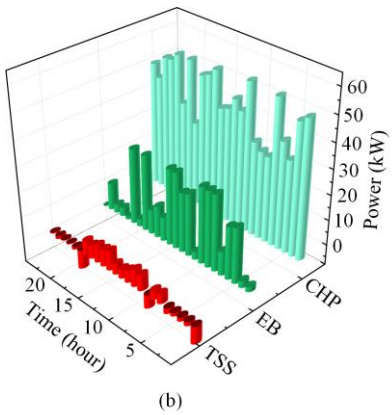

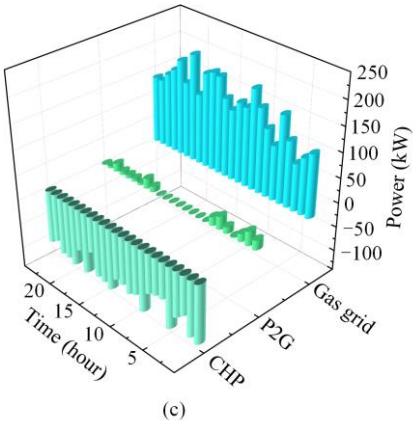

Fig. 10. Energy dispatch results in Case 3. (a) Electrical energy. (b) Thermal energy. (c) Natural gas.

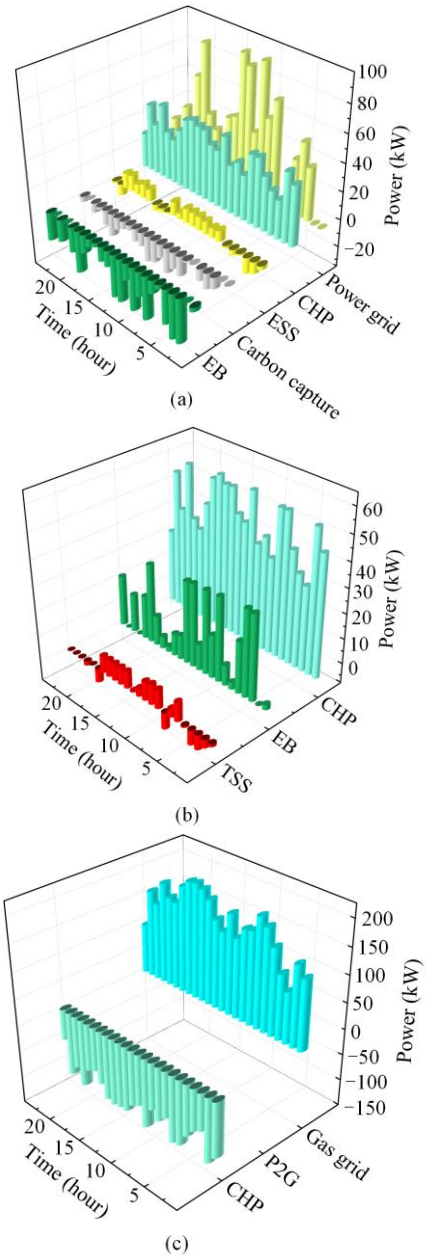

Fig. 11. Energy dispatch results in Case 4. (a) Electrical energy. (b) Thermal energy. (c) Natural gas.

To analyze the optimization results, this paper conducts a comparative analysis of Cases 2–4 against Case 1 (i.e., Figs. 8–11, and Tables IV and V), which serves as the baseline for evaluation.

1) Comparison Analysis of Optimization Results Between Case 2 and Case 1

In contrast to Case 1, Case 2 experiences heightened energy dispatch costs, diminished energy dispatch efficiency, and reduced capability for assimilating for wind power consumption, due to the absence of multi-element energy storage systems. The specific aspects of such performance are described as follows.

Figure 9(a) shows that, without the time-shifting capability of electrical energy provided by the ESS, the power output of the grid intensifies, and the grid supplies additional power for the RIES, even during peak electricity consumption hours (i.e., 10:00–13:00, and 14:00–15:00). At the same time, since the output of power grid positively correlates with the carbon capture energy consumption, there is a consequential surge in carbon capture energy consumption. This, in turn, triggers an increase in both the electrical energy interaction cost and environmental cost.

Figure 9(b) demonstrates that, in the absence of the time-shifting capability of thermal energy facilitated by the TSS, the output energy fluctuation of the EB is higher compared to Case 1. Besides, to compensate for the thermal load, the output of the CHP is increased, highlighting the challenges in maintaining a stable thermal supply.

Figure 9(c) underscores the significance of multi-element energy storage systems in enabling flexible energy utilization. In the absence of such systems, the inability to store and dispatch energy as needed results in a heightened demand for external natural gas, which subsequently drives up purchase costs. This highlights the importance of energy storage in optimizing resource allocation and reducing operational expenses.

2) Comparison Analysis of Optimization Results Between Case 3 and Case 1

In the absence of carbon capture device, Case 3 exhibits a lower energy dispatch cost than Case 1, albeit with a limited capability to consume wind power. The specific aspects of such performance are described as follows.

Figure 10(a) illustrates that for Case 3, the electrical energy consumption of the carbon capture device is 0, resulting in a complete elimination of environmental cost. However, the high dependence of the RIES on the power grid increases the cost of electrical energy interaction.

Figure 10(b) depicts that the EB assumes a greater role in thermal energy supply, thereby reducing the thermal energy output requirements of the CHP.

Figure 10(c) shows a notable decrease in the natural gas consumption of the CHP, together with an increase in natural gas production via the P2G technology. This reduces the dependence on external natural gas, leading to a reduction in the cost of purchasing natural gas from outside suppliers. However, the absence of carbon capture devices, which would typically provide free CO_2 for the P2G, results in an increase in the CO_2 purchase cost.

3) Comparison Analysis of Optimization Results Between Case 4 and Case 1

Compared to Case 1, Case 4 exhibits a lower energy dispatch cost in the absence of P2G. However, the energy output of Case 4 experiences significant fluctuations, and its capability to absorb wind power remains limited. The specific aspects of such performance are described as follows.

Figure 11(a) indicates that the power grid reduces its energy output to the RIES, leading to a corresponding decrease in the energy consumption of carbon capture devices. However, this adjustment results in more pronounced fluctuations in the output energy of the power grid.

Figure 11(b) reveals that both the CHP and EB exhibit significant fluctuations in their thermal energy outputs.

Figure 11(c) shows that to meet the gas load, the RIES increases its natural gas purchases. Additionally, due to the fluctuation of the output energy of the CHP, the natural gas network also produces large fluctuations when transmitting natural gas to the RIES.

In summary, although Case 4 has the lowest total cost, its wind power consumption capability is the worst which is only 92.45%. Case 2 has a high wind power consumption capability of 98.03%, but its total cost is the highest. Case 3 has a low total cost, and at the same time, its wind power consumption capability is 98%, showing good overall performance. Case 1, despite increasing certain economic costs, has the strongest wind power consumption capability of 100%, demonstrating excellent comprehensive performance. Evidently, although the proposed model (i.e., Case 1) sacrifices economy to some extent, it can fully utilize renewable energy, enhance the carbon reduction capability of the integrated energy system, and reduce carbon environmental pollution. Meanwhile, experimental results also prove that combining carbon capture devices with P2G equipment is an effective way to reuse CO_2 as a resource.

D. Comparison of Environmental Pollution Degree for RIESs

The excessive emission of CO_2 poses detrimental impacts on our planet, such as accelerating of global warming, which in turn leads to increased temperatures, rising sea-levels, and disruption of ecological balance. Consequently, in this section, a comparative analysis of the carbon environment pollution degree of the RIESs in Cases 1–4 is conducted. Here, the carbon environment pollution level of the RIESs is indicated by the CRC of the system, where a stronger CRC signifies a lower degree of carbon environmental pollution, while a weaker CRC indicates a higher level of pollution.

The CRC of RIESs is given as follows:

$$C_{\mathrm{crc}}=\left(\sum_{t=1}^{T}(W_{\mathrm{c}}(t))/\sum_{t=1}^{T}\begin{pmatrix}\eta_{\mathrm{f}}\times(P_{\mathrm{oc}}(t)+P_{\mathrm{p}\to\mathrm{c}}(t))+\\ \eta_{\mathrm{g}}\times P_{\mathrm{g}\to\mathrm{c}}(t)\end{pmatrix}\right)\times 100\% \tag{31}$$

where C_{crc} represents the CRC of RIESs, and η_{g} represents CO_2 generated coefficient for consuming natural gas.

To compare and analyze the carbon environmental pollution degree of the RIESs, the total generation, and the capture and emissions of CO_2 from the RIESs for Cases 1–4, are described. The results are shown in Fig. 12, while the re-utilization rate of captured CO_2 and the carbon reduction capability of the RIESs are shown in Table VI.

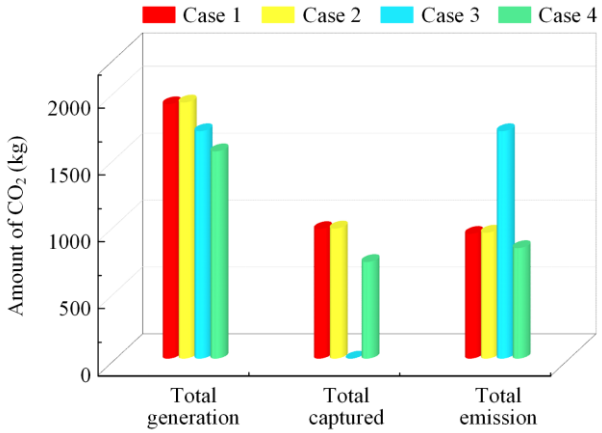

Fig. 12. Total generation, capture and emission of CO_2 from the RIESs in Cases 1–4.

TABLE VI
REUTILIZATION RATE OF CAPTURED CO_2 AND CARBON REDUCTION CAPABILITY OF THE RIES IN EACH CASE

Cases	1	2	3	4
Re-utilization rate of captured CO_2 (%)	4.50	3.52	0	0
Carbon reduction capability of RIESs (%)	50.95	50.81	0	46.64

Similarly, the carbon environmental pollution degree of the RIES in Case 1 serves as the benchmark for comparison, against which the carbon environmental pollution degree of the RIESs in Cases 2–4 are analyzed.

Case 2 vs. Case 1. The dependence of Case 2 on external energy leads to higher total CO_2 emission, result-

ing in lower utilization and carbon reduction capabilities for captured CO_2 in Case 2 compared to Case 1.

Case 3 vs. Case 1. Although the total generation amount of CO_2 in Case 3 is low, the absence of carbon capture devices leads to high CO_2 emission and low carbon reduction capability. Meanwhile, because P2G cannot recycle this part of CO_2, there is a conflict between high CO_2 emission and zero CO_2 utilization rate.

Case 4 vs. Case 1. The total generation, capture and emissions of CO_2 in Case 4 decrease. However, the high dependence on natural gas in Case 4 results in a reduced carbon reduction capability. Meanwhile, there is no P2G environment to resourcefully reuse the captured CO_2, resulting in its zero re-utilization rate.

In summary, the model proposed in this paper can improve the carbon reduction capacities of RIESs and mitigate carbon environment pollution by optimizing energy utilization. Moreover, the combination of carbon capture devices and P2G equipment offers an efficient way for the secondary utilization of CO_2.

VI. Comparative Analysis of Algorithms

To verify the soundness of the proposed ASCOSNPS-based method, it is compared with the GA and QPSO alternatives, under the same situation. Likewise, Case 1 is employed as the experimental subject, while the accuracy, number of iterations, and optimization results achieved by these algorithms are compared.

A. Comparative Analysis of the Accuracy of the Algorithms

The comparison results on accuracy are shown in Table VII, where the accuracy rate is expressed as follows:

$$\lambda_{\mathrm{r}} = \frac{Q_{\mathrm{r}}}{Q_{\mathrm{sum}}} \tag{32}$$

where λ_{r} represents the accuracy rate, Q_{sum} represents the number of experiments (taken as 10000 in the paper), and Q_{r} represents the number of experimental results satisfying the given constraints.

TABLE VII
ACCURACY OF ASCOSNPS, GA AND QPSO

Algorithms	ASCOSNPS	GA	QPSO
Accuracy rate (%)	99.92	99.91	98.97

It can be seen from Table VII that, despite the good results of the three algorithms, the accuracy of ASCOSNPS is slightly higher than those of GA and QPSO. This shows that the ASCOSNPS-based method can effectively deal with high-dimensional problems and avoid the constrained imbalance problem slightly better than other approaches.

B. Comparative Study of the Number of Iterations

In this section, the results on the convergence of the different methods along the iterations are analyzed and compared in Fig. 13. It illustrates that the ASCOSNPS-based method has a lower objective function value (i.e., a lower minimum economic cost of energy dispatch) with respect to GA, which has the highest (i.e., the worst) objective function value and is very easy to fall into local optimal solutions in the iterations. While QPSO has the lowest objective function value, it requires the highest number of iterations (i.e., 420 iterations), whereas ASCOSNPS completes the optimization process within 312 iterations.

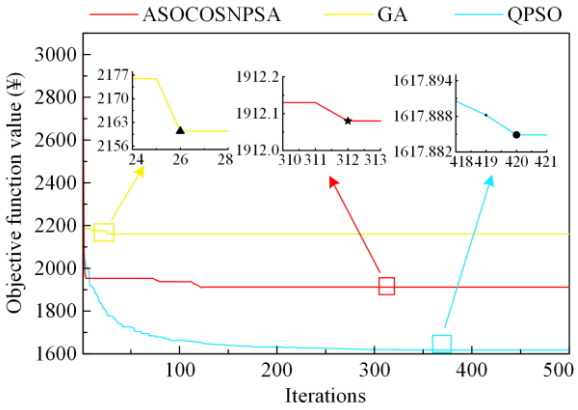

Fig. 13. Iteration of ASCOSNPS, GA and QPSO.

C. Comparative Analysis of the Optimization Results

In order to verify the competitiveness of the ASCOSNPS-based method in optimizing the proposed model (i.e., ETG-RIES), the comparative results of the aforementioned three algorithms are shown in Table VIII.

Specifically, we observe that GA enables the ETG-RIES to reduce the dependence on natural gas, but it increases CO_2 emissions by 25.79%. Moreover, although the amount of CO_2 captured under GA is the highest, its re-utilization rate is lower than the one under the ASCOSNPS-based method. Furthermore, the carbon reduction capability of the ETG-RIES under GA is also low.

The ETG-RIES operating under QPSO exhibits significantly lower carbon reduction capability and wind power consumption rates compared to the ASCOSNPS-based method. This is due to the large amount of natural gas purchased from the external market, which is converted into electrical and thermal energy by the CHP. This kind of energy conflicts with the wind power consumption, resulting in the wind power not being fully absorbed. Besides, despite QPSO achieving the lowest CO_2 emissions, the re-utilization rate of the captured CO_2 remains at a mere 0.05%, failing to harness the full potential of integrating carbon capture devices with the P2G equipment.

TABLE VIII
OPTIMIZATION RESULTS OF ASCOSNPS, GA AND QPSO

Algorithms	Natural gas purchased (kWh)	CO_2 captured (kg)	CO_2 emissions (kg)	Re-utilization rate of CO_2 captured (%)	Carbon reduction capability of ETG-RIES (%)	Consumption rate of wind power (%)
ASCOSNPS	3754.98	969.80	933.75	4.50	50.95	100
GA	3242.21	1205.13	1174.56	2.99	50.64	100
QPSO	4129.76	548.95	810.77	0.05	40.37	87.76

In summary, the ASCOSNPS-based method surpasses both GA and QPSO in terms of the overall and comprehensive performance. While achieving 100% wind power consumption, the ASCOSNPS-based method not only improves the carbon reduction capability of the ETG-RIES but also mitigates its carbon environmental pollution to a greater extent.

VII. CONCLUSIONS

Within the context of RIES and low-carbon energy scheduling, a mathematical framework-based model for the ETG-RIES is proposed, abstracting its core components. The model adopts various energy conversion equipment and a multi-element energy storage system to enhance the flexibility of energy scheduling. Besides, the connection of carbon capture devices and P2G equipment provides a viable path to reuse CO_2 and realize the reduction of carbon emission.

Meanwhile, to effectively optimize the proposed ETG-RIES model, a novel ASCOSNPS-based method is proposed, which introduces the cumulative mutation operator and the adaptive mutation operator. It shows that the ASCOSNPS-based method can not only escape local optima in the search for an optimal solution in a high-dimensional problem, but also balance the contribution of the penalty function and avoid the constraint imbalance. Furthermore, the results of this study show the followings:

1) The proposed ETG-RIES adopts the MESS that takes into account the immediate response speed of charging and discharging. This technology can flexibly utilize energy through the feature of energy time-shifting, realizing 100% consumption of wind power with uncertain factors. Furthermore, the MESS can store energy when energy prices are low and use energy when prices are high, which allows for saving in energy consumption costs and maximizing the functional and economic value of the energy storage system.

2) Although the carbon capture devices increase the energy scheduling cost of the ETG-RIES, they significantly reduce CO_2 emission. The experimental results show that the ETG-RIES can reduce the CO_2 emission by around 45% compared to the RIES without carbon capture devices.

3) P2G can not only effectively consume wind power, but also reuse the CO_2 captured by the carbon capture device as the raw material for synthetic natural gas for secondary utilization.

4) Compared with GA and QPSO, the proposed ASCOSNPS-based method shows its superiority in the accuracy rate, the re-utilization rate of CO_2 captured, the carbon reduction capability of the ETG-RIES, and the consumption rate of wind power.

In summary, both the ETG-RIES and ASCOSNPS-based method have good performances in the carbon reduction capability. The ETG-RIES can satisfy with the diversified energy use demand, and soften the rigid connection between the energy and the loads. At the same time, the proposed operation optimization method achieves the optimal purpose of the ETG-RIES, based on which the reduction of CO_2 emission and deep consumption of wind power are achieved.

This study focuses on the theoretical model building and simulation verification. Future work will explore opportunities to apply the proposed theoretical framework in real-world environments, directly demonstrating the effectiveness and potential issues of the method and providing valuable feedback and directions for improvement.

ACKNOWLEDGMENTS

Not applicable.

AUTHORS' CONTRIBUTIONS

Tao Wang: formal analysis, investigation, supervision, writing-review & editing, and data curation. Zhu Huang: formal analysis, investigation, writing-original draft and data curation. Ruixuan Ying: writing-original draft and data curation. Luis Valencia-Cabrera: writing-review & editing. All authors read and approved the final manuscript.

FUNDING

This work is partially supported by the National Natural Science Foundation of China (No. 61703345) and the Chunhui Project Foundation of the Education Department of China (No. Z201980).

AVAILABILITY OF DATA AND MATERIALS

Not applicable.

DECLARATIONS

Competing interests: The authors declare that they have no known competing financial interests or personal relationships that could have appeared to influence the work reported in this article.

AUTHORS' INFORMATION

Tao Wang received the Ph.D. degree in electrical engineering at the Southwest Jiaotong University, Chengdu, China, in 2016. She worked as a visit student in the computer science and artificial intelligence, University of Seville, Seville, Spain, during Nov. 2013 to Nov. 2014. She was a lecturer in the Xihua University, China (2017–2019). She has published 1 book, over 30 invention patents and more than 84 papers. She has been selected as the world's top 2% scientists for three years (2020, 2021 and 2023), whose sub-field is energy under the field of artificial intelligence & image processing. She is currently an associate professor in the School of Electrical Engineering and Electronic Information at the Xihua University since 2019. Also, she is the subdecanal of the School of Electrical Engineering and Electronic Information at Xihua University. She is now a backup candidate for academic and technical leaders in Sichuan province. Her research interests include artificial intelligence and its application in electrical power systems.

Zhu Huang received the M.S. degree in the Xihua University, China, in 2022. She is currently working in the China Yangtze Power Co., Ltd. since 2022. Her research interests include integrated energy systems and spiking neural P systems.

Ruixuan Ying received the bachelor's degree in the Xihua University, China, in 2022. He is currently studying for a M.S. degree in the Tohoku university, Japan. His research interests include machine learning, optimization algorithms, computer vision, natural language processing, magnetic physics, and AI for science.

Luis Valencia-Cabrera received his Ph.D. degree in logics, computing, and artificial intelligence from the University of Seville in 2015. He also earned multiple M.S. degrees in related fields from the University of Seville and Andalusia Business Confederation + Sun Microsystems between 2007 and 2013. He was a researcher (2010–2011), lecturer (2011–2019) and senior lecturer (2019–2022) at the University of Seville and has held various academic and professional positions. He is currently an associate professor in the Department of Computer Science and Artificial Intelligence at the University of Seville since 2022. His research interests include artificial intelligence, natural computing, and the application of AI in complex systems.

REFERENCE

[1] X. Zhao, H. Yin, and Y. Zhao, "Impact of environmental regulations on the efficiency and CO2 emissions of power plants in China," *Applied Energy*, vol. 149, pp. 238-247, 2015 .

[2] Z. Han , G. Na, and H. Dong *et al*., "Robust optimal operation of integrated energy system with P2H considering flexibility balance," *Power System Protection and Control*, vol. 51, no. 6, pp. 161-169, Mar. 2023. (in Chinese)

[3] Y. Qiu, Q. Li, and Y. Ai *et al*., "Two-stage distributionally robust optimization-based coordinated scheduling of integrated energy system with electricity-hydrogen hybrid energy storage," *Protection and Control of Modern Power Systems*, vol. 8, no. 2, pp. 1-14, Apr. 2023.

[4] A. R. Azzam and D. Ibrahim, "Development and assessment of an integrated wind-solar based energy system for sustainable communities," *Energy Conversion and Management*, vol. 277, 2023.

[5] J. Ye and R. Yuan, "Integrated natural gas, heat, and power dispatch considering wind power and power-to-gas," *Sustainability*, vol. 9, no. 4, Feb. 2017.

[6] W. Li, T. Li, and H. Wang *et al*., "Optimal dispatch model considering environmental cost based on combined heat and power with thermal energy storage and demand response," *Energies*, vol. 12, no. 5, Sep. 2019.

[7] S. Yu, J. Horing, and Q. Liu *et al*., "CCUS in China's mitigation strategy: insights from integrated assessment modeling," *International Journal of Greenhouse Gas Control*, vol. 84, pp. 204-218, 2019.

[8] W. Sun, J. Wu , and Q. Zhang, "Coordinated optimization of a distribution network and multi-integrated energy microgrid based on a double-layer game," *Power System Protection and Control*, vol.52, no. 2, pp. 26-38, Jan. 2024. (in Chinese)

[9] Y. Li, Y. Zou, and Y. Tan *et al*., "Optimal stochastic operation of integrated low-carbon electric power, natural gas and heat delivery system," *IEEE Transactions on Sustainable Energy*, vol. 9, no. 1, pp. 273-283, Jan. 2018.

[10] L. He, Z. Lu, and J. Zhang *et al*., "Low-carbon economic dispatch for electricity and natural gas systems considering carbon capture systems and power-to-gas," *Applied Energy*, vol. 224, pp. 357-370, 2018.

[11] M. A. Hossain, H. R. Pota, and S. Squartini *et al*., "Modified PSO algorithm for real-time energy management in grid-connected microgrids," *Renewable Energy*, vol. 136, pp. 746-757, 2019.

[12] Q. Wen, G. Liu, and W. Wu *et al*., "Genetic algorithm-based operation strategy optimization and multi-criteria evaluation of distributed energy system for commercial buildings," *Energy Conversion and Management*, vol. 226, 2020.

[13] M. Qin, Y. Yang, and X. Zhao *et al.*, "Low-carbon economic multi-objective dispatch of integrated energy system considering the price fluctuation of natural gas and carbon emission accounting," *Protection and Control of Modern Power Systems*, vol. 8, no. 4, pp.1013-1030, Oct. 2023.

[14] G. Zhang, H. Rong, and F. Neri *et al.*, "An optimization spiking neural P system for approximately solving

combinatorial optimization problems," *International Journal of Neural Systems*, vol. 24, no. 5, Article number 1440006 (16 pages), 2014.

[15] J. Dong, G. Zhang, and B. Luo *et al*., "A distributed adaptive optimization spiking neural P system for approximately solving combinatorial optimization problems," *Information Sciences*, vol. 596, pp. 1-14, 2022.

[16] Z. Wei, S. Zhang, and G. Sun *et al*., "Power-to-gas considered peak load shifting research for integrated electricity and natural-gas energy systems," *Proceedings of the CSEE*, vol. 37, no. 16, pp. 4601-4609, Aug. 2017. (in Chinese)

[17] C. Stephen and M. Pierluigi, "Integrated modeling and assessment of the operational impact of power-to-gas (P2G) on electrical and gas transmission networks," *IEEE Transactions on Sustainable Energy*, vol. 6, no. 4, pp. 1234-1244, Apr. 2015.

[18] W. Liu, Z. Li, and Y. Yang *et al*., "Collaborative optimal configuration for integrated energy system considering uncertainties of demand response," *Automation of Electric Power Systems*, vol. 44, no. 10, pp. 41-53, May 2020. (in Chinese)

[19] Z. Ji, C. Kang, Q. Chen *et al*., "Low-carbon power system dispatch incorporating carbon capture power plants," *IEEE Transactions on Power Systems*, vol. 28, no. 4, pp. 4615-4623, Apr. 2013.

[20] S. Zhou, W. Zhuang and Z. Wu *et al*., "Optimal Stochastic of multi-region gas and power complementary system considering tiered gas tariff," *Energy*, vol. 193, pp. 197-221, 2020.

[21] H. Liu, Z. Feng, and J. Wang *et al*., "Economic dispatch of integrated energy systems considering conditional value-at-risk," *Power System Technology*, vol. 42, no. 5, pp. 1385-1392, May 2018. (in Chinese)

[22] W. Liu, F. Wen, and Y. Xue, "Power-to-gas technology in energy systems: current status and prospects of potential operation strategies," *Journal of Modern Power Systems and Clean Energy*, vol. 5, no. 3, pp. 439-450, May 2017.

[23] Y. Song, Y. Wang, and J. Yi, "Microgrid energy source optimization planning considering demand side response and thermo-electrical coupling," *Power System Technology*, vol. 42, no. 11, pp. 3469-3476, Nov. 2018. (in Chinese)

[24] Z. Wang, Y. Shi, and Y. Tang *et al*., "Low carbon economy operation and energy efficiency analysis of integrated energy systems considering LCA energy chain and carbon trading mechanism," *Proceedings of the CSEE*, vol. 39, no. 6, pp. 1614-1626, Mar. 2019. (in Chinese)

[25] Y. Cui, P. Zeng, and X. Liu *et al*., "Low-carbon economic dispatch of electro-gas-thermal integrated energy system based on oxy-combustion technology," *Proceedings of the CSEE*, vol. 41, no. 2, pp. 592-607, Jan. 2021.

[26] J. Dong, S. Nie, and H. Huang *et al*., "Research on economic operation strategy of CHP microgrid considering renewable energy sources and integrated energy demand response", *Sustainability*, vol. 11, no. 18, pp. 1-22, Sep. 2019.